Journal of Machine Construction and Maintenance
QUARTERLY 1/2018(108)
ISSN 1232-9312
p. 7–15

Vijay Bhooshan KUMAR
Institute of Nanotechnology and Advanced Materials, Department of Chemistry, Bar-Ilan University, Ramat-Gan, Israel

Zeev PORAT
Division of Chemistry, Nuclear Research Center-Negev, Be'er-Sheva, Israel

Aharon GEDANKEN
Institute of Nanotechnology and Advanced Materials, Department of Chemistry, Bar-Ilan University, Ramat-Gan, Israel
gedanken@mail.biu.ac.il; vijaybhushan86@gmail.com

IMPROVED PHOTOVOLTAIC PROPERTIES OF A BACK-CONTACT ELECTRODE PRODUCED BY COPPER DEPOSITION ON CARBON-DOTS/CARBON PAPER

Key words: back contact; carbon-dots, carbon-paper, electrodeposition of copper.

Abstract: The implementation of carbon dots in electronic devices are among the hot topics in today's research. The current work describes the fabrication of a new back contact electrode for solar cells with the modification of carbon paper by the uniform deposition of highly crystalline carbon dots (CD). The ~5nm size CD were synthesized by the sonication of polyethylene glycol (PEG-400), which was further deposited on carbon paper. Copper was successfully electrodeposited onto the modified C-dots carbon-paper (C-paper@CD) through a potentiostatic procedure. The SEM and XRD results show that the electrodeposition of copper on CD-modified carbon paper is denser than pristine carbon-paper. A detailed study of CD@C-paper and Cu/Cu_2O-CD@C-paper was performed using the XRD, SEM, Raman, EDS, Elemental mapping, KPFM (Kelvin Probe Force Microscope), etc. The as-prepared electrode comprising of a C-paper modified with CD was tested in solar cells as a back contact, and it demonstrated superior high photo-voltage, significantly useful for photovoltaic implications.

Ulepszone właściwości fotowoltaiczne dolnej warstwy kontaktowej wytwarzanej metodą depozycji miedzi na skojarzeniu kropki węglowe/papier węglowy

Słowa kluczowe: elektroda dolna, kropki węglowe, papier węglowy, elektrodepozycja miedzi.

Streszczenie: Implementacja kropek węglowych w zastosowaniach elektronicznych to obecnie jeden z najszybciej rozwijających się kierunków współczesnej nauki. W artykule opisano nową metodę wytwarzania dolnej warstwy kontaktowej (elektrody dolnej) w ogniwach fotowoltaicznych techniką równomiernej depozycji wysoce krystalicznych kropek węglowych (CD). CD wielkości ~5 nm generowano poprzez sonikację glikolu polietylenowego (PEG-400), który deponowano na papierze węglowym. Na tak zmodyfikowanym papierze (C-paper@CD) miedź osadzano metodą potencjostatycznej elektrodepozycji. Wyniki analiz SEM oraz XRD wskazują, że zastosowana technologia sprzyja powstawaniu bardziej zwartych warstw przewodzących w porównaniu z niemodyfikowanym papierem węglowym. Szczegółowe badania CD@C-paper oraz skojarzenia Cu/Cu_2O-CD@C-paper przeprowadzono z wykorzystaniem technik XRD, SEM, spektroskopii Ramana, EDS, mapowania elementarnego, KPFM (mikroskopia sił z sondą Kelvina) i innych. Wytworzone elektrody były także testowane w ogniwach słonecznych w roli dolnej warstwy kontaktowej i wykazały wybitne właściwości szczególnie pożądane w zastosowaniach fotowoltaicznych.

Introduction

During the past three decades, carbon materials have been investigated as an extremely versatile product that exists in numerous forms with diverse chemical, electrical, physical, and electrochemical properties [1, 2]. Nanometric carbon materials have recently emerged as a unique class of optical nanomaterials targeting both biomedical and energy conversion applications [3–7]. As newly emergent carbon materials, carbon dots (C-dots) have attracted considerable research interest due to their superior optical properties,

excellent biocompatibility, small size, and low cost of production [8–12]. These fascinating physical properties are responsible for a wide range of the potential applications of C-dots [4, 11–14], such as solar cells [15], nanoelectronic devices [8], photodynamic therapy [16, 17], gene delivery [18], and as photocatalysts [19].

Generally, copper is used as an electrode in many electronic devices, because of its stability and conductivity [20]. CuO is also used as an interlayer in many electrochemical devices [21]. Cuprous oxide (Cu_2O) is a p-type semiconductor that has attracted increasing attention in recent years as an active component in solar cells and photodiodes, due to its narrow band gap (2.0–2.2 eV), high absorption efficiency over the wavelength range of the solar spectrum, low preparation cost, and non-toxicity [22–24]. Cuprous oxide has been synthesized by several methods, including thermal oxidation, anodic oxidation, chemical reduction of copper salt (such as $Cu(OH)_2$, $CuSO_4$ and $CuAc_2$), sol–gel chemistry, and a variety of gas-phase deposition techniques.

The current research is employing the sonochemical deposition method for coating carbon paper with C-dots. The sonochemical coating technique was used for the depositing a large variety of nanoparticles on surfaces such as ceramics, polymeric, metallic, glasses, textiles, and paper. Recently, we have described a simple method for producing C-dots by the prolonged sonication of polyethylene glycol (PEG) 400 [25].

The hybrid perovskite $CH_3NH_3PbI_3$ is among the leading photovoltaic materials that have been extensively studied in the last few years [26–28]. The implication of $CH_3NH_3PbI_3$ perovskite materials have recently emerged as arguably the most promising of all next generation thin film solar cell technologies. $CH_3NH_3PbI_3$ organic inorganic hybrid perovskites can be processed in solution or evaporated at low temperatures to form simple thin-film photojunctions, thus delivering the potential for the holy grail of high efficiency, low embedded energy, and low cost photovoltaics that are in progress [29–31]. Among flexible electronic devices, the design of a conductive flexible electrode is challenging, because it includes both a flexible front and back electrode. The optical and electronic properties of the flexible film can be tuned by doping the electrode material with other elements [32].

In this study, economically viable, the facile sonochemical synthesis method [24] is employed for the *in situ* formation of C-dots from polyethylene glycol (PEG). Subsequent to their formation, the sonochemical coating method was adapted for coating the C-paper with C-dots and Cu_2O/Cu. The synthesis of C-dots does not require a strong acid, base, volatile organic solvent, or other post-synthetic surface passivation. Our procedure includes a preliminary step in which the carbon paper is first modified with C-dots (CD@C--paper). On the coated carbon paper, a layer of copper is electrodeposited. The presence of the carbon dots helped in the electrodeposition process. The main goal of this study is to design a back contact electrode for solar cells as well as for flexible electronic devices. We have tested the performance of /CD@C-paper electrode material in solar cells as a back contact, and it was found that the work function of the CD@C-paper is higher when compared with pristine C-paper, demonstrating superior photo voltage in the solar cell device.

1. Experimental

1.1. Chemicals

Polyethylene glycol (99.998%), H_2SO_4, $CuSO_4{\cdot}5H_2O$, and $Cu(COOCH_3)_2$ were purchased from Sigma-Aldrich and used as received. The carbon paper was purchased from FuellCellsEtc (USA).

1.2. Experimental procedure

CD were prepared as follows: 20 mL of polyethylene glycol (PEG-400) were transferred into a test tube which was dipped in a water bath at 75°C as described in our previous work [25, 37]. Ultrasonic irradiation was applied for 2.5 h using an ultrasonic transducer (Sonics and Materials Inc., USA, model VCX 750, 20 kHz, 230 V AC) at 70% amplitude. Upon sonication, C-dots were obtained as a suspension in PEG that was cooled down to room temperature. Then a piece of C-paper (1x1cm) was inserted into the suspension of the C-dots in PEG-400, and the sonication was continued for 4 hours at lower amplitude (25%) in an ice bath. The as-prepared carbon paper modified with C-dots (CD@C-paper) was washed with ethanol and water to remove excess PEG-400 and dried in a vacuum. Electrodeposition of Cu_2O/Cu onto the CD@C-paper was done from a solution that contained 249 g/L copper sulphate ($CuSO_4{\cdot}5H_2O$), 70 g/L H_2SO_4, and 102 g/L $CuAc_2$.

Electrochemical measurements: The current density–voltage curves were measured in a perovskite solar cells with a configuration of FTO/TiO_2 blocking layer/ mesoporous TiO_2/$CH_3NH_3PbI_{2-x}Cl_x$/Spiro-Ome AD/Back electrode. A piece of a CD@C-paper with a layer of electrodeposited Cu/Cu_2O was used as a back electrode. In order to simulate a full solar cell, we placed this carbon paper electrode on Spiro OMeTAD (2,2',7,7'-Tetrakis-(N,N-di-4-methoxyphenylamino)-9,9'-spirobifluorene) and pressed with contact during current-voltage measurements in order to avoid loose contact.

1.3. Analytical equipment

The fluorescence of the C-dots was measured by a Varian Cary Eclipse fluorescence spectrophotometer.

A high resolution transmission electron microscopy (HRTEM) study was carried out using a JEOL 2100 microscope operated at 200 kV. A high resolution scanning electron microscope (HRSEM) imaging was done with a FEI Megallon 400L microscope, operated at 20 kV. Elemental analysis and elemental mapping were performed using HRSEM Energy Dispersive X-ray Spectroscopy (EDS). The Raman spectra of C-paper and CD@C-paper were recorded by a Renishaw inVia Raman microscope equipped with RL785 and RL830 Class 3B wavelength-stabilized diode lasers and a Leica DM2500 M (Leica Microsystems) microscope. Kelvin probe force *(KPFM) imaging*: Potential QNM (PeakForce™ Quantitative potential mapping) was done by using a Bio FastScan Scanning Probe Microscope (Bruker corp., USA). FastScan-C cantilevers (Bruker) with spring constants 0.45 N/m were used.

1.4. The Work function measurement

The KPFM measures contact potential differences (CPD) between a conducting AFM tip and a sample. The CPD between the tip and a sample is defined as follows:

$$V(cpd) = \frac{\varphi tip - \varphi sample}{-e}$$

Whereas φ_{sample} and φ_{tip} are the work functions of the sample and tip, and e is the electronic charge. When an AFM tip is brought close to the sample surface, an electrical force is generated between the tip and the sample surface, due to the differences in their Fermi energy levels.

2. Results and discussions

2.1. Synthesis of C-dots (CD) and their deposition on carbon paper by the sonochemical method

C-dots were formed by the sonication of PEG--400 for 2.5 h. at 75°C and 70% sonication amplitude, as reported in our previous works [25, 37]. The fluorescence emitted from the C-dots formed in the supernatant solution was recorded at different excitation wavelengths (330, 350, 370, 390, 410, 430, and 450 nm). The emission curves are presented in Fig. 1a, showing the strongest emission intensity for excitation at 370 nm.

HRTEM image (Fig. 1b) shows that the typical size of the C-dots is ca. 3–8 nm and, the crystal lattice of the C-dots can be observed with d-spacing estimated as 0.21 nm. The size distribution of C-dots was plotted for a population of about 200 particles, which yielded a narrow size distribution curve that peaked at 5 nm (Fig. 1c). A SEM image of a section of untreated C-paper is represented in Fig. 1d, showing a disordered network of carbon fibres.

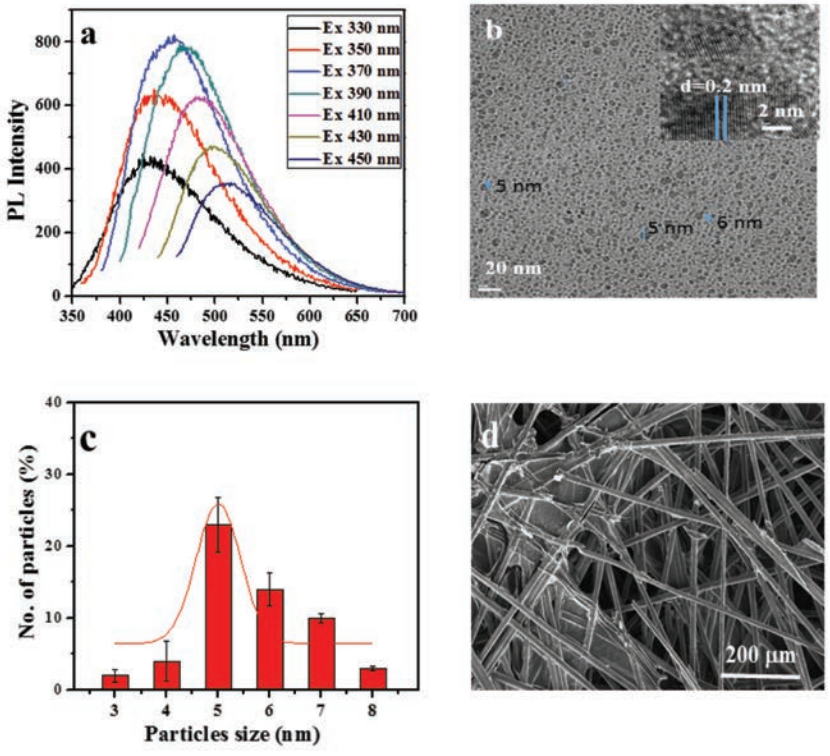

Fig. 1. a) Fluorescence spectra of C-dots for various excitation wavelengths, b) HRTEM image of the C-dots, c) Size-distribution curve of C-dots, d) HRSEM image of pristine carbon-paper

The C-dots modified carbon paper was analysed by Raman spectroscopy and compared to pristine carbon paper. In general, the spectra (Fig. 2) are similar to those of graphite, demonstrating two main signals at 1582 cm^{-1} (G-band) and at 2707 cm^{-1}. The signal at 1354 cm^{-1} (D-band) is rather diminished for pristine C-paper but is considerably intense for the C-paper coated with C-dots. The band at 1354 cm^{-1} reflects the properties of carbon dots. Moreover, the small signal at 2942 cm^{-1} in the spectrum of the C-dots modified carbon paper is appearing due to modification of C-paper by C-dots. The Raman band at 2942 cm^{-1} that is detected only in the CD@C-paper originates from a double resonance process that links phonons to the electronic band structure, [38, 39] and it confirms the presence of D+G bands of graphene or, in other words, the presence of C-dots on the C-paper.

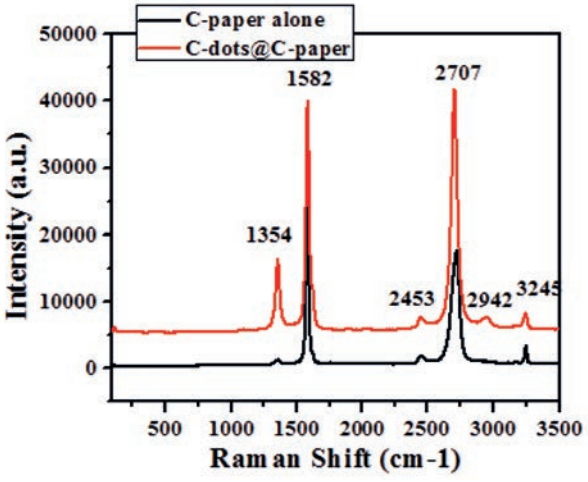

Fig. 2. Raman spectra of C-paper alone (red line) and CD@C-paper (black line)

2.2. Electrodeposition of copper on carbon paper

Electrodeposition of copper on 1×1 cm^2 pieces of carbon paper was performed according to the procedure described in the experimental section using 1M aqueous solutions of either $CuSO_4$ or $Cu(CH_3CO_2)_2$. The same results were obtained for both copper salts. The dried samples were examined by X-ray diffraction and showed similar diffraction patterns for the products obtained from either salt solution. The diffractograms for the pristine C-paper and CD@C-paper samples, before and after copper deposition, are presented in Fig. 3. Before deposition, only the major phase of graphite is observed at 2θ=26°, together with a tiny signal at 2θ=54°, which is also due to the graphitic nature of carbon. After deposition of the copper, the diffraction pattern includes four more diffraction peaks; three of them match the database for metallic copper, and the small diffraction peak at 2θ=37° is attributed to Cu_2O, which indicates partial oxidation of the deposited metallic copper.

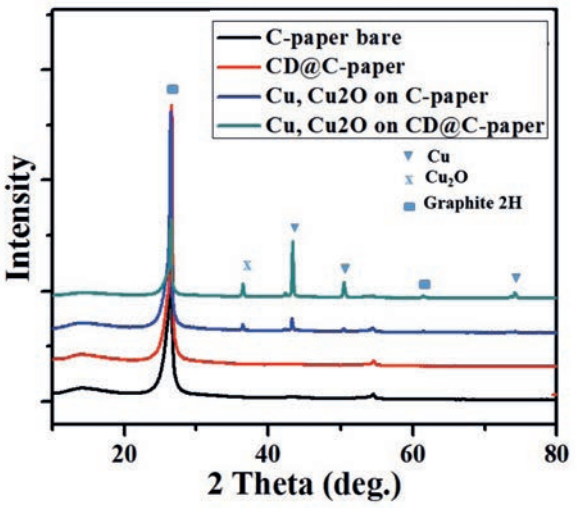

Fig. 3. XRD patterns of C-paper, CD@C-paper, C-paper and CD@C-paper with Cu/Cu_2O layer deposited on them electrochemically from 0.5 M $CuSO_4$ solution at room temperature

Visual examination of the copper deposits on C-paper and on CD@C-paper samples was obtained by HRSEM (Figs. 4 and 5).

The crystal shape of the copper is similar on both samples but the coverage is different, as can be seen in the lower-magnification images while the carbon fibers of the untreated carbon paper are only partially covered with copper, and full coverage was obtained on the C-dots modified carbon paper. Elemental analysis by EDS of the area is shown in Fig. 6.

The figure exhibits the presence of C, Cu, and O. The quantitative atomic ratio between the copper and oxygen is about 3:1; whereas, elemental mapping shows uniform distribution of these elements. These results imply that the surface of the copper crystallites is partially oxidized. It is worth noting the complementary nature of these images: In areas where no copper was deposited (and oxidized), the underlying carbon substrate is the dominant element.

The effect of time on the electrodeposition of Cu/Cu_2O on C-paper/CD@C-paper from $CuSO_4$ aq. solution was performed for 10 minutes as well as for 60 minutes. We characterized the electrodeposited Cu/Cu2O layers by XRD and Raman spectroscopy. The X-ray diffraction patterns show that, for 10 minutes of electrodeposition, le Cu/Cu_2O is deposited on C-paper/CD@C-paper (This interpretation is made on the basis of intensity of XRD and HRSEM analysis). On the basis of XRD and SEM analysis, it is concluded that similar amounts are deposited for 30 and 60 minutes (Fig. 7).

Therefore, the optimum deposition time is 30 minutes. Raman spectra measured from C-paper and C-dots/C-paper with Cu_2O electrodeposits are shown in Fig. 8.

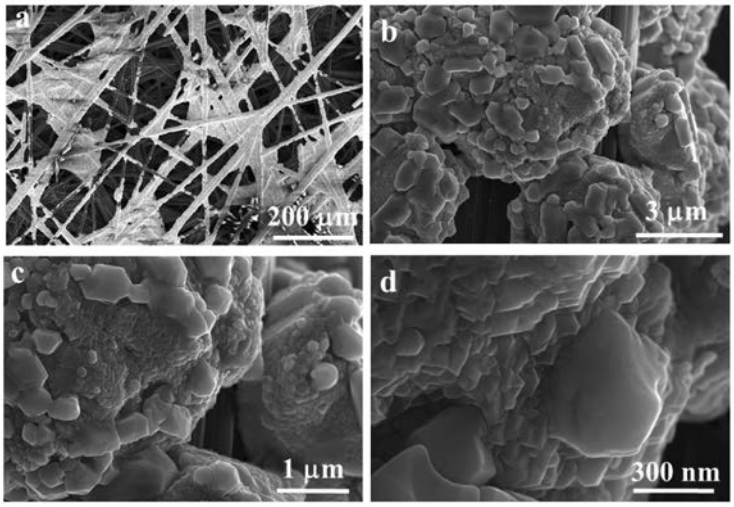

Fig. 4. HRSEM images at four magnifications of Cu/Cu_2O electrodeposited on CD@C-paper from 0.5 M $CuSO_4$ solution: a) 200 µm, b) 3 µm, c) 1 µm, d) 300 nm

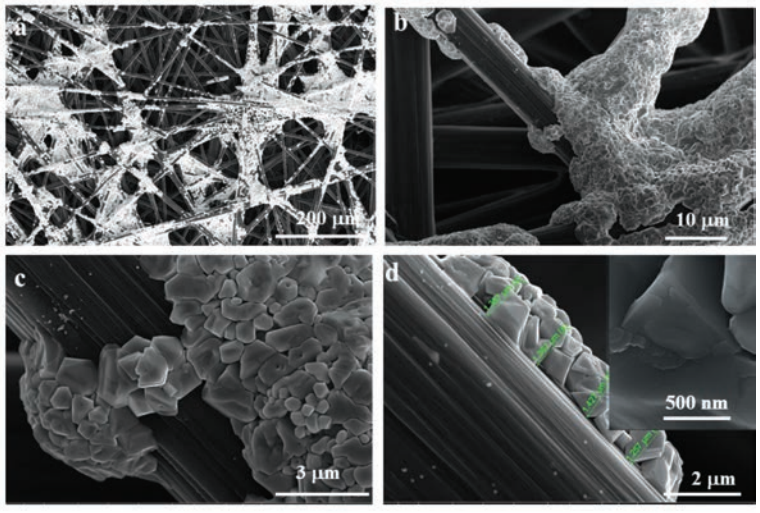

Fig. 5. HRSEM images at four magnifications (as indicated) of Cu electrodeposited on C-paper from 0.5 M $CuSO_4$ solution: a) 200 µm, b) 10 µm, c) 3 µm, d) 2 µm/500 nm

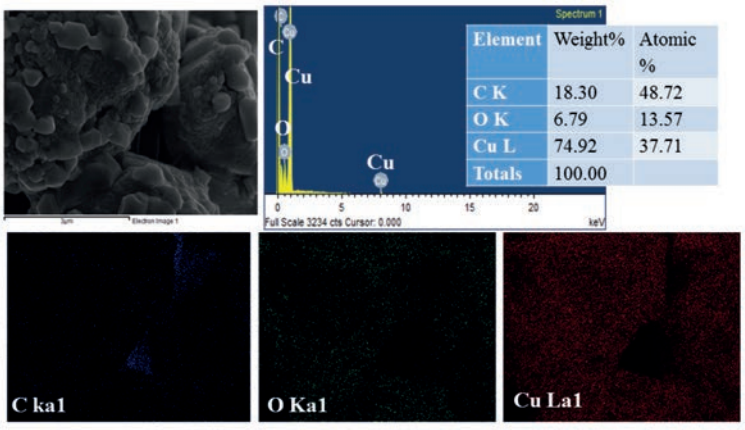

Fig. 6. HRSEM images with EDS and elemental mapping of Cu/Cu_2O deposited on C-paper by electrodeposited for 2000 s at potentials of 0.5 using $CuSO_4$ aq. soln.

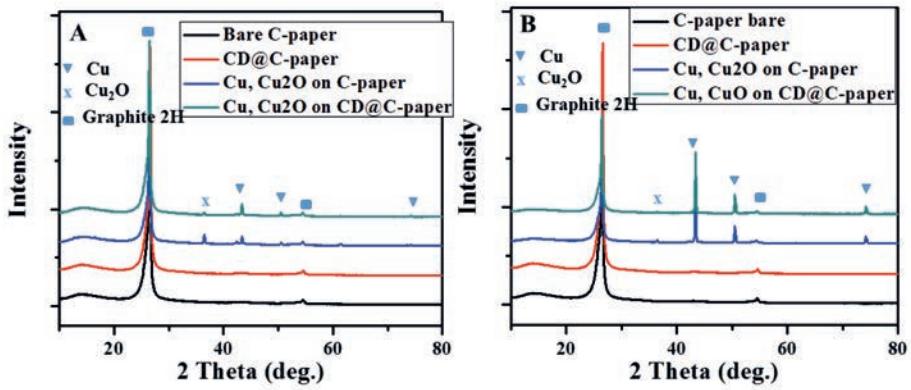

Fig. 7. XRD patterns of C-paper, CD@C-paper, Cu/Cu_2O deposited on C-paper/CD@C-paper by electrodeposition for (A) 10 minutes (B) 60 minutes)

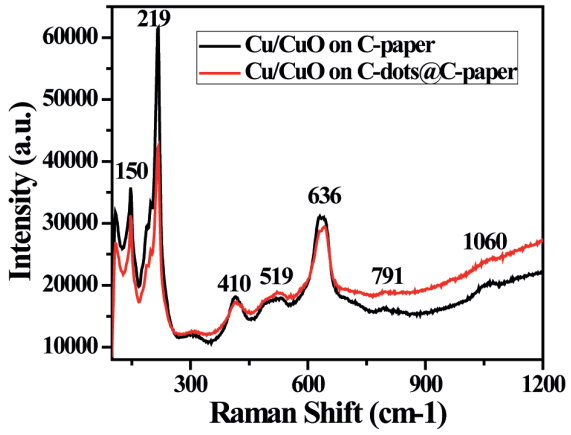

Fig. 8. Raman spectra of Cu/Cu_2O deposited on C-paper/ CD@C-paper by electrodeposited for 30 minutes

Identical Raman spectra of Cu/Cu_2O were obtained for the Cu/Cu_2O deposited on modified C-paper and pristine C-paper, which implies that both samples contain the Cu/Cu_2O. The Raman peak at 636 cm^{-1} corresponds to Cu_2O.

2.3. Electrochemical deposition and energetic modification of carbon paper by carbon dot and Cu/CuO

Effect of back contact on solar cells: We have tested the as prepared electrode comprising of C-paper@C-dots with electrodeposited Cu/Cu_2O electrode in solar cells as a back contact. Generally, a solar cell consists of two metal electrodes: the transparent front electrode and the back metal electrode.

Figure 9 demonstrates the current-voltage curves measured from perovskite solar cells. A device with only carbon paper as a back-contact shows 810 mV_{oc}, the C-dot/C-paper displays shows open circuit voltage of 890 mV; however, the Cu/CuO@C-dot/C-paper displays highest open circuit voltage of 985 mV and a current of 180 µA. The differences in the voltage generation in these two devices could arise from the changes in the energetic levels or the surface area of the modified carbon paper, which is further supported by work function measurements. The carbon paper modified with C-dots has a higher work function, whose Fermi level is close to the valance band (VB) of spiro, which reveals less voltage loss; therefore, the device shows higher V_{oc} compared to unmodified carbon paper. However, the Cu/Cu_2O coating has a similar work function, since it can be oxidised very easily and becomes less conductive. This could be one of the reasons for the lower voltage measured from a solar cell. The Cu/Cu_2O

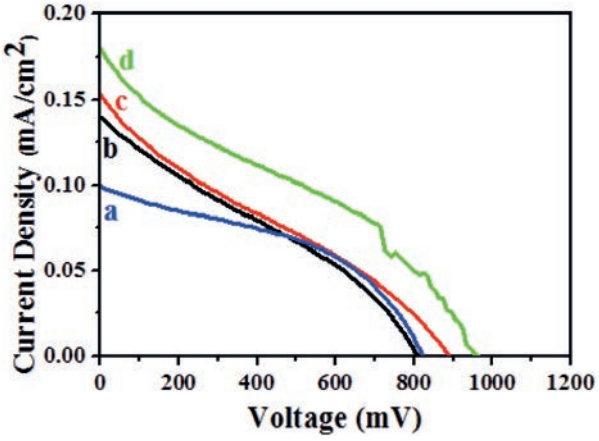

Fig. 9. Current density – Voltage curves measured from perovskite solar cells comprising of various electrodes as back contact: (a) bare carbon paper, (b) carbon paper modified with C-dots, (c) carbon paper with electrodeposited Cu/Cu_2O, and (d) carbon paper modified with C-dots on which copper was deposited for 30 min.

deposit on C-paper and on CD@C-paper gives the very low voltage, which could be due to the poor quality of contact at the interface, the formation of a thick oxide layer, or possibly some other electronic process that decreases the performance of the solar cells. For detailed understanding, further study needs to be done.

The work function of the Cu/Cu_2O on C-paper and on CD@C-paper was measured by the help of Kelvin probe force microscopy (KPFM). Figure 10 shows the energy level diagram of the tip and the sample surface when φ_{sample} and φ_{tip} are different. Figure 10a depicts the potential profile of Cu/Cu_2O@CD@C-paper energy levels of the interface between deposited Cu/Cu_2O and CD@C-paper. Figure 10c represents the potential profile of Cu/Cu_2O and CD@C-paper. Figure 10b shows the topography of the Cu/Cu2O deposited on the CD@C-paper and depicts homogeneous distribution of Cu/Cu_2O. Figure 10d just captured the optical imaged covered by the camera during the measurement of potential by KFM. Equilibrium requires Fermi levels to line-up at steady state, if the tip and the sample surface are close enough for electron tunnelling. Upon electrical contact, the Fermi levels will align through electron current flow, and the system will reach an equilibrium state, Fig. 10c. The tip and sample surface will be charged, and an apparent VCPD (voltage applied to contact potential difference) will form (Note: the Fermi energy levels are aligned but vacuum energy levels are no longer the same, and a VCPD between the tip and sample has formed). The difference in the work function of the materials Cu/Cu_2O and CD@C-paper was found to be 75 meV. However, the work function of copper metal is 4.5 eV, which suggest that Cu/Cu_2O@CD@C--paper is the best candidate for a back contact for solar cells devices.

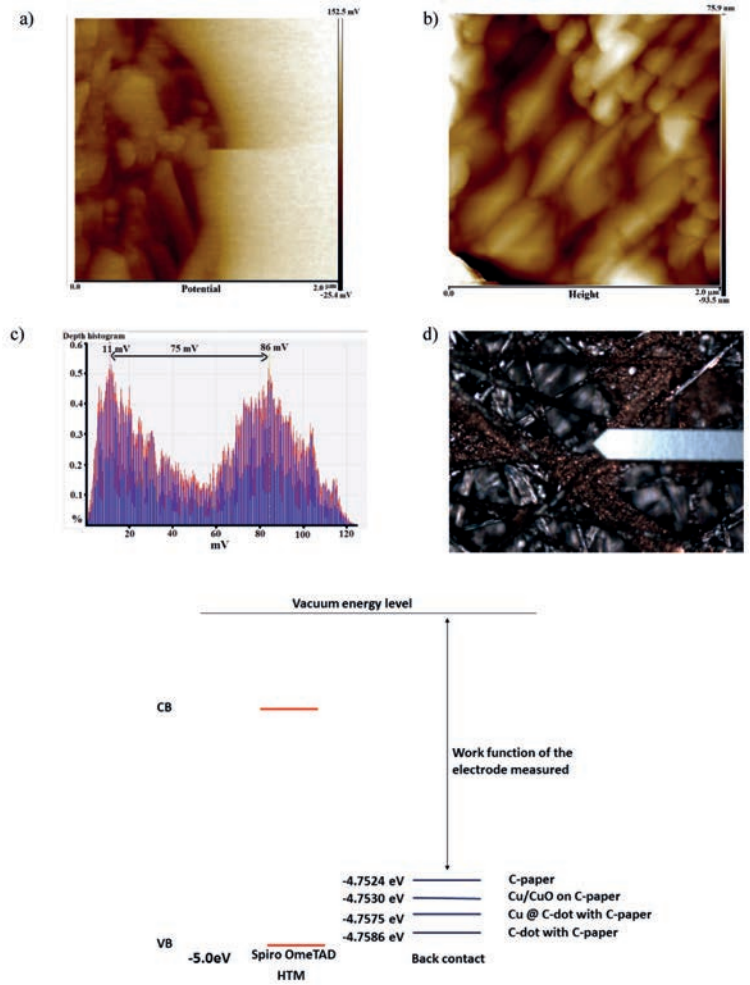

Fig. 10. a) Potential profile of Cu/Cu_2O@CD@C-paper, b) Height profile of Cu/Cu_2O@CD@C-paper, c) Potential measurement on the basis of fig. 10a, d) optical images of KPFM tip and sample during the measurement

Conclusions

In conclusion, a straightforward sonochemical approach is employed for the *in situ* formation of C-dots via ultrasonic irradiation of polyethylene glycol (PEG) solvent. The synthesis does not require a strong acid, base, volatile organic solvent, or other post-synthetic surface passivation. Our procedure includes a preliminary step in which the carbon paper is first modified with C-dots (CD@C-paper), which improves the electrodeposition of copper on it. The goal of this paper is to design a new electrode for solar cell applications. We demonstrated that CD@C-paper can be implemented as back contact in solar cells. It has better performance than the carbon paper, and these results correlate with the energetic changes of work function, which we observed in photo voltage measurements of the device.

Acknowledgement

The authors are grateful to Mr. Laxman Gouda of the Department of Chemistry, Bar-Ilan University, for his help with the back contact measurement.

References

1. Shenderova O. A., Zhirnov V.V., Brenner D.W. (2002) Carbon Nanostructures. Crit Rev Solid State Mater Sci 27:227–356. doi: 10.1080/10408430208500497.
2. Dai L. (2006) Chapter 1 From conventional technology to carbon nanotech- nology : The fourth industrial revolution and the discoveries of C ^ Q , carbon nanotube and nanodiamond.
3. Hu S., Zhao Q., Dong Y., et al (2013) Carbon-dot-loaded alginate gels as recoverable probes: Fabrication and mechanism of fluorescent detection. Langmuir 29:12615–12621. doi: 10.1021/la402647t.
4. Shen L., Chen M., Hu L., et al (2013) Growth and stabilization of silver nanoparticles on carbon dots and sensing application. Langmuir 29:16135––16140. doi: 10.1021/la404270w.
5. Lv L., Fan Y., Chen Q., et al (2014) Three-dimensional multichannel aerogel of carbon quantum dots for high-performance supercapacitors. Nanotechnology 25:235401. doi: 10.1088/0957-4484/25/23/235401.
6. Chen Q., Hu Y., Hu C., et al (2014) Graphene Composites for High-Performance. Phys Chem Chem Phys 16:19307–19313. doi: 10.1039/C4CP02761b.
7. Gao S., Chen Y., Fan H., et al (2014) A green one-arrow-two-hawks strategy for nitrogen-doped carbon dots as fluorescent ink and oxygen reduction electrocatalysts. J Mater Chem A 2:6320. doi: 10.1039/c3ta15443b.
8. Tan M., Zhang L., Tang R., et al (2013) Enhanced photoluminescence and characterization of multicolor carbon dots using plant soot as a carbon source. Talanta 115:950–956. doi: 10.1016/j.talanta.2013.06.061.
9. Yin B., Deng J., Peng X., et al (2013) Green synthesis of carbon dots with down- and up-conversion fluorescent properties for sensitive detection of hypochlorite with a dual-readout assay. Analyst 138:6551–6557. doi: 10.1039/C3AN01003A.
10. Barati A., Shamsipur M., Arkan E., et al (2015) Synthesis of biocompatible and highly photoluminescent nitrogen doped carbon dots from lime: Analytical applications and optimization using response surface methodology. Mater Sci Eng C 47:325–332. doi: 10.1016/j.msec.2014.11.035.
11. Prasannan A., Imae T. (2013) One-pot synthesis of fluorescent carbon dots from orange waste peels. Ind Eng Chem Res 52:15673–15678. doi: 10.1021/ie402421s.
12. Li C.-L., Ou C.-M., Huang C.-C., et al (2014) Carbon dots prepared from ginger exhibiting efficient inhibition of human hepatocellular carcinoma cells. J Mater Chem B 2:4564–4571. doi: 10.1039/C4TB00216D.
13. Kozák O., Datta K.K.R., Greplová M., et al (2013) Surfactant-derived amphiphilic carbon dots with tunable photoluminescence. J Phys Chem C 117:24991–24996. doi: 10.1021/jp4040166.
14. Mehta V.N., Jha S., Kailasa S.K. (2014) One-pot green synthesis of carbon dots by using Saccharum officinarum juice for fluorescent imaging of bacteria (Escherichia coli) and yeast (Saccharomyces cerevisiae) cells. Mater Sci Eng C 38:20–27. doi: 10.1016/j.msec.2014.01.038.
15. Bian J., Huang C., Wang L., et al (2014) Carbon dot loading and TiO_2 nanorod length dependence of photoelectrochemical properties in carbon dot/TiO_2 nanorod array nanocomposites. ACS Appl Mater Interfaces 6:4883–90. doi: 10.1021/am4059183.
16. Bourlinos A.B., Trivizas G., Karakassides M.A., et al (2015) Green and simple route toward boron doped carbon dots with significantly enhanced non-linear optical properties. Carbon N Y 83:173–179. doi: 10.1016/j.carbon.2014.11.032.
17. Hu S., Tian R., Dong Y., et al (2013) Preparation and optical properties of phthalocyanine–carbon dot blends. RSC Adv 3:21447. doi: 10.1039/c3ra42090f.
18. Dou Q., Fang X., Jiang S., et al (2015) Multi-functional fluorescent carbon dots with antibacterial and gene delivery properties. RSC Adv 5:46817–46822. doi: 10.1039/c5ra07968c.

19. Li H., Kang Z., Liu Y., Lee S.-T. (2012) Carbon nanodots: synthesis, properties and applications. J Mater Chem 22:24230. doi: 10.1039/c2jm34690g.
20. Kim W.-K., Lee S., Hee Lee D., et al (2015) Cu mesh for flexible transparent conductive electrodes. Sci Rep 5:10715. doi: 10.1038/srep10715.
21. Gao X., Aikawa S., Mitoma N., et al (2014) Self--formed copper oxide contact interlayer for high-performance oxide thin film transistors. Appl Phys Lett. doi: 10.1063/1.4890312.
22. Olsen L.C., Bohara R.C., Urie M.W. (1979) Explanation for low-efficiency Cu2O Schottky-barrier solar cells. Appl Phys Lett 34:47–49. doi: 10.1063/1.90593.
23. Wang L.C., de Tacconi N.R., Chenthamarakshan CR, et al (2007) Electrodeposited copper oxide films: Effect of bath pH on grain orientation and orientation-dependent interfacial behavior. Thin Solid Films 515:3090–3095. doi: 10.1016/j.tsf.2006.08.041.
24. Tu J., Yuan Y., Jiao H., Jiao S. (2014) RSC Advances electrodeposition onto carbon paper and its. 16380––16384. doi: 10.1039/c4ra00592a.
25. Kumar V.B., Porat Z., Gedanken A. (2016) Facile One-Step Sonochemical Synthesis of Ultrafine and Stable Fluorescent C-dots. Ultrason Sonochem 28:367–375. doi: 10.1016/j.ultsonch.2015.08.005.
26. Bhooshan Kumar V., Gouda L., Porat Z., Gedanken A. (2016) Sonochemical synthesis of CH3NH3PbI3 perovskite ultrafine nanocrystal sensitizers for solar energy applications. Ultrason Sonochem 32:54–59. doi: 10.1016/j.ultsonch.2016.02.012.
27. Jang D.M., Park K., Kim D.H., et al (2015) Reversible Halide Exchange Reaction of Organometal Trihalide Perovskite Colloidal Nanocrystals for Full-Range Band Gap Tuning. Nano Lett 150714104303009. doi: 10.1021/acs.nanolett.5b01430.
28. Kamat P.V. (2013) Evolution of perovskite photovoltaics and decrease in energy payback time. J Phys Chem Lett 4:3733–3734. doi: 10.1021/jz402141s.
29. Lin Q., Armin A., Burn P.L., Meredith P. (2016) Organohalide Perovskites for Solar Energy Conversion. Acc Chem Res 49:545–553. doi: 10.1021/acs.accounts.5b00483.
30. Albero J., Malik A.R., Garcia H. (2016) Influence of the Composition of Hybrid Perovskites on their Performance in Solar Cells. J Mater Chem A 4353––4364. doi: 10.1039/C6TA00334F.
31. Kutes Y., Zhou Y., Bosse J.L., et al (2016) Mapping the Photoresponse of CH3NH3PbI3 Hybrid Perovskite Thin Films at the Nanoscale. Nano Lett 1–28. doi: 10.1021/acs.nanolett.5b04157.
32. Abdelhady A.L., Saidaminov M.I., Murali B., et al (2016) Heterovalent Dopant Incorporation for Bandgap and Type Engineering of Perovskite Crystals. J Phys Chem Lett 7:295–301. doi: 10.1021/acs.jpclett.5b02681.
33. Gedanken A. (2004) Using sonochemistry for the fabrication of nanomaterials. Ultrason Sonochem 11:47–55. doi: 10.1016/j.ultsonch.2004.01.037.
34. Jost K., Perez C.R., McDonough J.K., et al (2011) Carbon coated textiles for flexible energy storage. Energy Environ Sci 4:5060. doi: 10.1039/c1ee02421c.
35. Hu L., La Mantia F., Wu H., et al (2011) Lithium-ion textile batteries with large areal mass loading. Adv Energy Mater 1:1012–1017. doi: 10.1002/aenm.201100261.
36. Harifi T., Montazer M. (2015) A review on textile sonoprocessing: A special focus on sonosynthesis of nanomaterials on textile substrates. Ultrason Sonochem 23:1–10. doi: 10.1016/j.ultsonch.2014.08.022.
37. Kumar V.B., Perelshtein I., Lipovsky A., et al (2015) The sonochemical synthesis of Ga@C-dots particles. RSC Adv 5:25533–25540. doi: 10.1039/C5RA01101A.
38. Li Y., Zhong X., Rider A.E., et al (2014) Fast, energy-efficient synthesis of luminescent carbon quantum dots. Green Chem 16:2566–2570. doi: 10.1039/C3GC42562B.
39. Li Y., Zhao Y., Cheng H., et al (2012) Nitrogen-doped graphene quantum dots with oxygen-rich functional groups. J Am Chem Soc 134:15–18. doi: 10.1021/ja206030c.